

Novel Preparation Methods for the Fabrication of Thin-Film EXAFS Samples

M.C. Ridgway¹, C.J. Glover^{1,*}, P. Kluth¹, B. Johannessen¹ and G.J. Foran²

¹*Department of Electronic Materials Engineering, Australian National University, Canberra, Australia*

²*Australian Synchrotron Research Program, Australian Nuclear Science and Technology Organisation, Menai, Australia*

Abstract. Thin-film EXAFS samples have been fabricated using semiconductor-processing and wet-chemical etching techniques to eliminate artifacts associated with transmission and fluorescence measurements. Examples include crystalline $\text{Ge}_x\text{Si}_{1-x}$ alloys, amorphous GaAs and Cu and Au nanocrystals in SiO_2 . In general, thin films of several microns thickness were first formed on bulk substrates then EXAFS samples were fabricated by separating the thin film and substrate. For transmission measurements, thin films were stacked together to yield the optimum absorption while sample inhomogeneity, non-uniformity and non-continuity were readily eliminated. For fluorescence measurements, scattering/diffraction from the substrate was eliminated and stacking the thin films together increased the areal concentration of the absorber. The use of such techniques to fabricate EXAFS samples yielded a significant increase in accessible photo-electron wave number range and hence more accurate structural parameter determinations.

Keywords: EXAFS, crystalline, amorphous, $\text{Ge}_x\text{Si}_{1-x}$, GaAs, metal nanocrystals, SiO_2 .

PACS: 61.10.Ht, 61.43.Dq, 61.46.Hk, 61.66.Dk

INTRODUCTION

Using EXAFS measurements to reliably and accurately determine structural parameters necessitates minimizing or eliminating artifacts associated with the sample. For example, transmission measurements can be plagued by particle-size and thickness effects in addition to sample inhomogeneity, non-uniformity and non-continuity. Similarly, fluorescence measurements can be hampered by self absorption and parasitic scattering/diffraction contributions to the solid-state detector total yield. For this report, we describe three examples of novel sample preparation methods for fabricating artifact-free thin-film EXAFS samples using a combination of semiconductor-processing and wet-chemical etching techniques.

METHODS, RESULTS AND DISCUSSION

Crystalline $\text{Ge}_x\text{Si}_{1-x}$ Alloys

The three bondlengths (Si-Si, Ge-Si and Ge-Ge) in $\text{Ge}_x\text{Si}_{1-x}$ alloys should exhibit behaviors intermediate between the Bragg-Pauling and Vegard extremes [1].

Equivalently, three separate bond lengths, each varying as a function of composition x , have been predicted. Given bulk $\text{Ge}_x\text{Si}_{1-x}$ alloys are not readily available, previous measurements have generally been performed in fluorescence mode using thin $\text{Ge}_x\text{Si}_{1-x}$ alloy layers deposited on bulk Si substrates [2,3]. Conflicting results have been reported and thus we sought to perform transmission measurements to extend the accessible photo-electron wave number (k) range. A series of $\text{Ge}_x\text{Si}_{1-x}$ alloy compositions of thickness $\sim 3 \mu\text{m}$ were deposited epitaxially on Si-on-insulator (Si ($0.1 \mu\text{m}$)/ SiO_2 ($1 \mu\text{m}$)/Si (bulk substrate)) wafers by molecular beam epitaxy. The $\text{Ge}_x\text{Si}_{1-x}$ alloy and Si overlayer were then separated from the bulk Si substrate by selective chemical etching of the SiO_2 layer with dilute HF. The thin $\text{Ge}_x\text{Si}_{1-x}$ /Si layer was then crushed and mixed with BN to yield the optimum thickness for transmission measurements at the Ge K-edge for each composition.

Figure 1 shows the Ge-Si and Ge-Ge bondlengths as a function of $\text{Ge}_x\text{Si}_{1-x}$ alloy composition [4]. Indeed the Ge-Ge bond length composition dependence closely matches theoretical predictions while the Ge-Si bond length exhibits a much lesser dependence on x . By separating the thin-film from the bulk substrate, transmission measurements were enabled. This eliminated the necessity of individual photon counting

with a solid-state detector in fluorescence mode and significantly extended the k range relative to previous measurements.

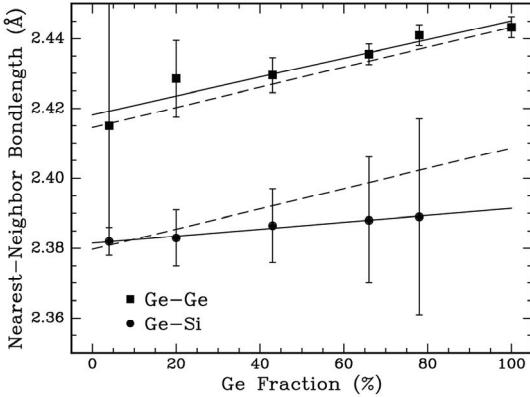


FIGURE 1. Ge-Si and Ge-Ge bondlengths as a function of composition x for $\text{Ge}_x\text{Si}_{1-x}$ alloys showing both experimental results [4] (solid lines) and theoretical predictions (dashed lines) [1].

Amorphous GaAs

Though lacking long-range order, amorphous compound semiconductors are expected to retain the short-range order characteristic of the crystalline phase [5] with both chemical disorder (homopolar bonding) and structural disorder (coordination defects plus bond length and bond angle distortion) potentially present. Transmission EXAFS measurements of amorphous GaAs (and other compound semiconductors) have typically been performed with non-stoichiometric samples resulting from the flash evaporation or sputtering processes used to deposit the amorphous material [6,7]. To negate such an effect, an epitaxial crystalline GaAs ($2.5 \mu\text{m}$)/AlAs ($0.02 \mu\text{m}$)/GaAs (bulk substrate) heterostructure was grown by metal organic chemical vapor deposition. Ion implantation was then utilized to amorphize the heterostructure to a depth of $\sim 3 \mu\text{m}$ and the amorphous GaAs overlayer was then separated from the bulk substrate by selective chemical etching of the AlAs layer with dilute HF. The continuous amorphous GaAs layers were then supported on adhesive Kapton and stacked together to yield the optimum thicknesses for transmission measurements at each of the Ga and As K-edges [8].

Figure 2 demonstrates the short-range order in amorphous GaAs [9]. The reconstructed inter-atomic depth distributions for both Ga and As absorbers are clearly asymmetric, skewed toward longer bondlengths, as characteristic of amorphous semiconductors in general [10]. (Though the similarity in photo-electron scattering from Ga and As

inhibited the identification of chemical disorder in amorphous GaAs, In-In bonding was readily quantifiable in amorphous InP [11].) Forming the amorphous thin-film with ion implantation eliminated non-stoichiometry and inhomogeneity while separating the thin-film from the substrate yielded continuous and planar EXAFS samples.

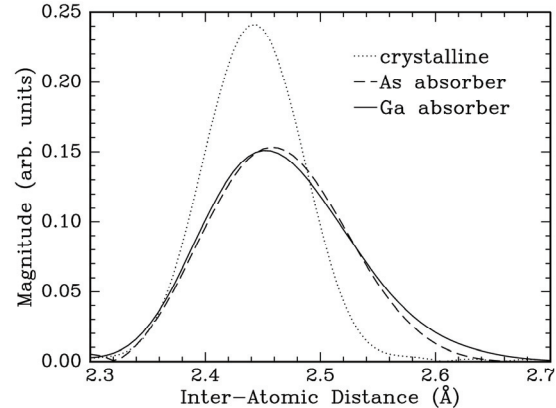


FIGURE 2. Inter-atomic distance distributions for both Ga and As absorbers in amorphous GaAs relative to a crystalline standard [9]. For the latter, spectra at the two edges were effectively identical and thus one is shown.

Cu and Au Nanocrystals in SiO₂

Finite-size effects in nanocrystals can yield structural perturbations relative to bulk crystalline material. For example, the curvature of a metal nanocrystal surface should result in a capillary pressure of GPa magnitude sufficient to induce a bond length contraction [12]. To study such an effect, Cu [13] and Au [14] nanocrystals of diameter 3-20 nm were formed in amorphous SiO₂ layers of thickness 2 μm on bulk Si substrates using ion implantation and thermal annealing. The bulk Si substrate was then removed by mechanical polishing and selective chemical etching using KOH and the nanocrystal-containing SiO₂ layers were stacked together, typically ten-fold, between Kapton.

Figure 3 shows the bond length contraction for Cu nanocrystals in SiO₂ as a function of inverse nanocrystal diameter [13] (where the latter was determined with small-angle x-ray scattering [15]). Except for the smallest nanocrystal size, the data is well fit with a linear function as consistent with a simple liquid-drop model [16]. Similar results were obtained for Au nanocrystals [14]. By removing the substrate, parasitic scattering/diffraction contributions were eliminated and by stacking the nanocrystal-containing thin films together, the areal concentration

of the absorber was increased by one order of magnitude. As a consequence, the metal absorber fluorescence signal comprised approximately one half of the incoming count rate to the solid-state detector and fluorescence measurements of very high quality were achievable.

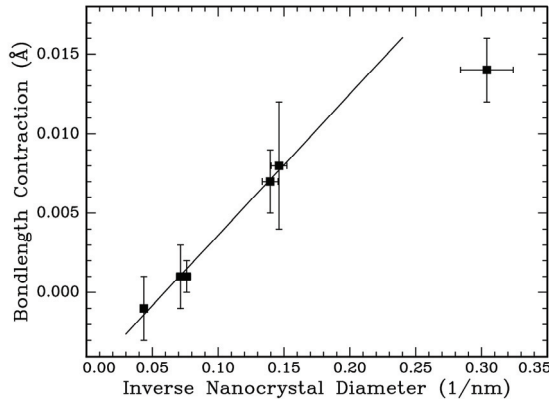


FIGURE 3. Bondlength contraction (relative to a bulk crystalline standard) as a function of inverse nanocrystal diameter for Cu nanocrystals in SiO₂ [13].

CONCLUSIONS

In summary, the use of semiconductor-processing and wet-chemical etching techniques can be of great benefit for the preparation of both transmission and fluorescence EXAFS samples. Common artifacts, and major sources of error, can be readily eliminated and more reliable and accurate EXAFS measurements can be performed. Furthermore, the methodologies described in this report for crystalline GexSi1-x alloys, amorphous GaAs and Cu and Au nanocrystals are readily extendable to many other materials systems.

ACKNOWLEDGMENTS

We thank the Australian Synchrotron Research Program, funded by the Commonwealth of Australia, and the Australian Research Council for financial

support. We also thank J.L. Hansen and H.H. Tan for growths by molecular beam epitaxy and metal organic chemical vapour deposition, respectively.

REFERENCES

1. N. Mousseau and M.F. Thorpe, Phys. Rev. **B46**, 15887 (1992).
2. D.B. Aldrich, R.J. Nemanich and D.E. Sayers, Phys. Rev. **B50**, 15026 (1994).
3. J.C. Woicik, K.E. Miyano, C.A. King, R.W. Johnson, J.G. Pellegrino, T.-L. Lee and Z.H. Lu, Phys. Rev. **B57**, 14592 (1998).
4. M.C. Ridgway, C.J. Glover, K.M. Yu, G.J. Foran, C. Clerc, J.L. Hansen and A. Nylandsted Larsen, Phys. Rev. **B60**, 10831 (1999).
5. E.P. O'Reilly and J. Robertson, Phys. Rev. **B34**, 8684 (1986).
6. J.A. Del Cueto and N.J. Shevchik, J. Phys. C: Sol. St. Phys. **11**, L829 (1978).
7. M.-L. Theye, A. Gheorghiu and H. Launois, J. Phys. C: Sol. St. Phys. **13**, 6569 (1980).
8. M.C. Ridgway, C.J. Glover, G. Foran and K.M. Yu, J. Appl. Phys. **83**, 4610 (1998).
9. M.C. Ridgway, G. de M. Azevedo, C.J. Glover, K.M. Yu and G.J. Foran, Nucl. Instrum. Meth. **B199**, 235 (2003).
10. M.C. Ridgway, C.J. Glover, G. de M. Azevedo, S.M. Kluth, K.M. Yu and G.J. Foran, Nucl. Instrum. Meth. **B238**, 294 (2005).
11. G. de M. Azevedo, C.J. Glover, M.C. Ridgway, K. M. Yu and G. J. Foran, Phys. Rev. **B68**, 115204 (2003).
12. R. Meyer, L.J. Lewis, S. Prakash and P. Entel, Phys. Rev. **B68**, 104303 (2003).
13. B. Johannessen, P. Kluth, C.J. Glover, G. de M. Azevedo, D.J. Llewellyn, G.J. Foran and M.C. Ridgway, J. Appl. Phys. **98**, 024307 (2005).
14. P. Kluth, B. Johannessen, V. Giraud, A. Cheung, C.J. Glover, G. de M. Azevedo, M.C. Ridgway and G.J. Foran, Appl. Phys. Lett. **85**, 3561 (2004).
15. B. Johannessen, P. Kluth, D.J. Cookson, G.J. Foran and M.C. Ridgway, Nucl. Instrum. Meth. **B246**, 45 (2006).
16. C.W. Mays, J.S. Vermaak and D. Kuhlmann-Wilsdorf, Surf. Sci. **12**, 134 (1968).

*current address: Australian Synchrotron Project, Clayton, Australia.